Direct capture in the ^{130}Sn$(n,\gamma)^{131}$Sn and ^{132}Sn$(n,\gamma)^{133}$Sn reactions under r-process conditions

Peter Mohr*
Diakonie-Klinikum, D-74523 Schwäbisch Hall, Germany, and
Institute of Nuclear Research (ATOMKI), H-4001 Debrecen, Hungary
(Received 4 November 2012; published 14 December 2012)

The cross sections of the ^{130}Sn$(n,\gamma)^{131}$Sn and ^{132}Sn$(n,\gamma)^{133}$Sn reactions are calculated in the direct capture model at low energies below 1.5 MeV. Using recent data from (d,p) transfer experiments on ^{130}Sn and ^{132}Sn, it is possible to avoid global input parameters with their inherent uncertainties and to determine all inputs to the direct capture model by local adjustments. The calculated direct capture cross sections of ^{130}Sn and ^{132}Sn are almost identical and have uncertainties of less than a factor of 2. The stellar reaction rates $N_A\langle\sigma v\rangle$ show a slight increase with temperature. Finally, an estimate for the influence of low-lying resonances to the stellar reaction rates is given.

DOI: 10.1103/PhysRevC.86.068803 PACS number(s): 24.50.+g, 25.40.Lw, 25.60.Tv, 26.30.−k

Direct capture (DC) is expected to be the dominating reaction mechanism if the level density in the compound nucleus is low. This is typically found for light and/or neutron-rich nuclei, especially with magic proton or neutron numbers, at low energies which is the relevant energy range for nuclear astrophysics. Direct neutron capture has been identified experimentally for several stable targets (e.g., ^{7}Li [1], ^{12}C [2], ^{16}O [3], ^{18}O [4,5], ^{22}Ne [6,7], ^{26}Mg [8,9], and ^{48}Ca [10,11]), but it is obvious that neutron capture experiments are practically impossible for short-living radioactive targets such as ^{130}Sn or ^{132}Sn. Thus, the determination of the DC cross section for unstable targets has to rely on theoretical predictions.

The calculation of DC cross sections requires several ingredients. First of all, the electromagnetic transition must be well defined. This requires the transition energy $E_\gamma = E + S_n - E_x$ and thus the neutron separation energy S_n (or the masses of the target and residual nucleus) and the excitation energy E_x of the final state. In addition, spin and parity J^π of the final state and its spectroscopic factor C^2S are essential ingredients for the calculation. Finally, the DC cross section depends on the square of the overlap integral

$$\mathcal{I} = \int dr\, u(r)\, \mathcal{O}^{E1}\, \chi(r), \tag{1}$$

where $\mathcal{O}^{E1}$ is the electric dipole operator and $u(r)$ and $\chi(r)$ are the bound-state wave function and scattering-state wave function. These wave functions are calculated from the two-body Schrödinger equation using a simple nuclear potential without an imaginary part because the damping of the wave function in the entrance channel by the tiny DC cross sections is very small [12]. The present study is restricted to $E1$ transitions, which are dominant in the DC cross section, whereas higher multipolarities such as $M1$ or $E2$ are practically negligible if dominant $E1$ transitions are allowed by the well-known electromagnetic transition rules [13]. Further details of the DC model can be found, e.g., in [8,10,12].

The cross sections of the ^{130}Sn$(n,\gamma)^{131}$Sn and ^{132}Sn$(n,\gamma)^{133}$Sn reactions play an important role in r-process nucleosynthesis. In general, the influence of neutron capture cross sections on r-process nucleosynthesis is relatively small because under typical conditions an equilibrium between (n,γ) and (γ,n) reactions is reached. However, during freeze-out the cross sections become important. This holds in particular for the ^{130}Sn$(n,\gamma)^{131}$Sn reaction because of the larger neutron separation energy $S_n = 5206 \pm 13$ keV of ^{131}Sn compared to the smaller $S_n = 2370 \pm 24$ keV for ^{133}Sn (taken from the latest mass evaluation [14]). A detailed study of r-process nucleosynthesis around $A \approx 130$ is given in [15]. The particular importance of the ^{130}Sn$(n,\gamma)^{131}$Sn cross section is highlighted in [16], and the most important temperature range is identified as $0.8 \leqslant T_9 \leqslant 1.3$ (where T_9 is the typical notation for the temperature in 10^9 K). This corresponds to thermal energies $70 \leqslant kT \leqslant 110$ keV. Because of the missing Coulomb barrier in neutron capture, the stellar reaction rate per mole and unit volume, $\mathcal{R}(T) = N_A\langle\sigma v\rangle$ (where the usual short term [reaction rate] will be used for $\mathcal{R}$ in the following), is mainly sensitive to the cross sections at energies around $E \approx kT$, and the temperature dependence of $\mathcal{R}(T)$ is small (e.g., for pure s-wave capture $\sigma \sim 1/v$ and $\mathcal{R}(T) = \text{const.}$).

Up to now, the DC cross sections of the ^{130}Sn$(n,\gamma)^{131}$Sn and ^{132}Sn$(n,\gamma)^{133}$Sn reactions have been calculated using global parametrizations of the required input parameters [13,17,18]. It was found that the DC cross section of the ^{130}Sn$(n,\gamma)^{131}$Sn reaction is very sensitive to the chosen parameters. At 30 keV a variation over three orders of magnitude is found (see Fig. 9 of [17]). The recent (d,p) experiments on ^{130}Sn [19] and ^{132}Sn [20] allow us for the first time to completely avoid global parametrizations. Instead, locally optimized parameters are used in this work for all ingredients of the DC calculation to minimize the resulting uncertainties.

I start with the analysis of the DC cross section for the doubly-magic ^{132}Sn target nucleus. The bound-state properties of the residual ^{133}Sn are well known from the ^{132}Sn$(d,p)^{133}$Sn experiment [20] and are summarized in Table I. The spectroscopic factors are compatible with unity (see Table I in [20]); thus, $C^2S \approx 1.0$ is adopted in the following calculations. Such

*WidmaierMohr@t-online.de

TABLE I. Properties of bound states in ^{131}Sn and ^{133}Sn (from [19–23]) and the considered $E1$ transitions.

J^π	E_x (keV)	E (keV)	C^2S	V_0 (MeV)	$L_i \to L_f$	
			^{131}Sn			
$3/2^+$	0	−5206	0.10	−39.40	1,3	2
$1/2^+$	332	−4874	0.10	−40.04	1	0
$5/2^+$	1655	−3551	0.10	−36.82	1,3	2
$7/2^-$	2628	−2578	0.70	−47.30	2,4	3
$3/2^-$	3404	−1802	0.70	−46.97	0,2	1
$1/2^-$	3986	−1220	1.00	−45.66	0,2	1
$5/2^-$	4655	−551	0.75	−43.70	2,4	3
			^{133}Sn			
$7/2^-$	0	−2370	≈1.0	−46.51	2,4	3
$3/2^-$	854	−1516	≈1.0	−45.93	0,2	1
$1/2^-$	1363	−1007	≈1.0	−44.74	0,2	1
$5/2^-$	2005	−365	≈1.0	−42.91	2,4	3

large spectroscopic factors are expected for single-particle states above the doubly-magic ^{132}Sn.

The nuclear potential is taken as the sum of a central and a spin-orbit potential,

$$V(r) = -V_0\, f(r) - V_{\rm LS}\, \frac{\rm fm^2}{r}\, \frac{df}{dr}\, \vec{L}\vec{S}, \qquad (2)$$

with the central depth V_0, the spin-orbit strength $V_{\rm LS}$, and the Woods-Saxon geometry

$$f(r) = \left[1 + \exp\left(\frac{r-R}{a}\right)\right]^{-1}, \qquad (3)$$

with the radius parameter $R = R_0 \times A_T^{1/3}$, $R_0 = 1.25$ fm, and $a = 0.65$ fm.

In a first step the bound-state wave functions $u(r)$ are calculated by adjusting the depth V_0 of the central potential (with $V_{\rm LS} = 0$) to the energy $E < 0$ (see Table I). With an additional spin-orbit potential, almost identical wave functions can be obtained using $V_0 = 45.5$ MeV (45.0 MeV) and $V_{\rm LS} = 18.6$ MeV (22.0 MeV) for the bound $L = 1$ ($L = 3$) states.

The second step is the calculation of the scattering wave function $\chi(r)$. The optical potential can be adjusted to experimental phase shifts for all partial waves or to the scattering length for the s wave. Unfortunately, such data are not available for the unstable nuclei under study. As an alternative, the potential strength can be adjusted to the energies of single-particle states (as already done for the bound-states above). For light nuclei often a significant parity dependence for the potential depth V_0 is found. However, with increasing mass this dependence decreases, and, e.g., for ^{49}Ca (above the doubly-magic ^{48}Ca) it is found that V_0 of the bound $L = 1$ states (derived from the bound-state energies) and V_0 of the s wave (derived from the scattering length) agree within about 1%. (This result is independent of details of the geometry of the potential; also for a folding potential the deviation is only about 1% [10]). Because of the minor difference of V_0 and $V_{\rm LS}$ for the $L = 1$ and $L = 3$ bound states, I adopt averages of $V_0 = 45.3$ MeV and $V_{\rm LS} = 20.3$ MeV for the calculation of the scattering wave functions $\chi(r)$.

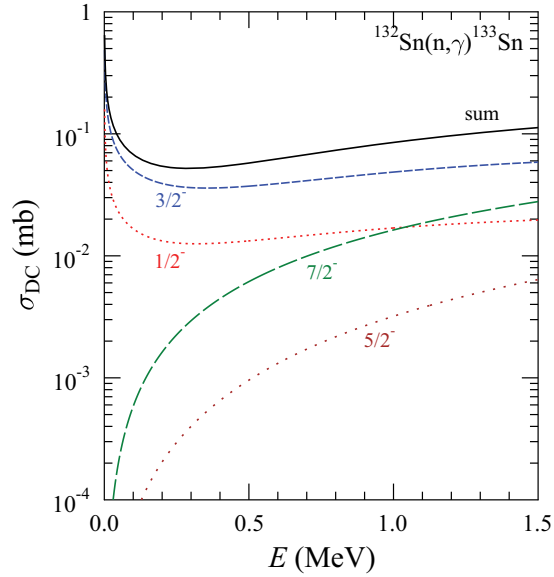

FIG. 1. (Color online) DC cross section of the ^{132}Sn$(n,\gamma)^{133}$Sn reaction. The contributions of the bound states in Table I are shown by colored dashed and dotted lines. The full black line represents the sum over all bound states.

Now all parameters for the calculation of the overlap integrals $\mathcal{I}$ in Eq. (1) are fixed by local adjustments to properties of ^{133}Sn = ^{132}Sn $\otimes\, n$, and the DC cross sections can be calculated without any further adjustments or parameters from global studies. The result for the ^{132}Sn$(n,\gamma)^{133}$Sn cross section is shown in Fig. 1. A discussion of uncertainties will be given later.

Exactly the same procedure is repeated for the ^{130}Sn$(n,\gamma)^{131}$Sn reaction. The bound-state properties of the $L = 1$ and $L = 3$ bound states are taken from the recent ^{130}Sn$(d,p)^{131}$Sn experiment [19]. Very similar to ^{133}Sn, no fragmentation of the levels has been found in ^{131}Sn, which is somewhat unexpected for the semi-magic ^{130}Sn core (compared to the doubly-magic ^{132}Sn core in the previous case). The resulting average parameters $V_0 = 46.2$ MeV and $V_{\rm LS} = 21.1$ MeV are derived from $V_0 = 46.6$ MeV (45.8 MeV) and $V_{\rm LS} = 20.3$ MeV (21.9 MeV) for the $L = 1$ ($L = 3$) bound states. The potential parameters remain very close to the data for ^{133}Sn and confirm the similarity of ^{131}Sn and ^{133}Sn.

The bound states with even parity are characterized by a particle-hole structure [19]. Thus, they have much smaller spectroscopic factors. These states are not suited for a determination of the potential depth V_0, which shows a broader spread. A spectroscopic factor of $C^2S = 0.1$ has been assumed for these states, which is in agreement with the upper limit of ≈0.3 given in [19] but somewhat lower than the average value of 0.347 for compiled spectroscopic factors [13,24]. The DC cross sections for the bound states with even parity are much smaller than those for the odd-parity bound states. The total DC cross section (summed over all transitions) does not depend strongly on the assumed value of $C^2S = 0.1$ for the weak transitions to the bound states with positive parity (see Fig. 2).

From the DC cross sections in Figs. 1 and 2 stellar reaction rates $\mathcal{R}(T) = N_A \langle \sigma v \rangle$ can be calculated. Note that the

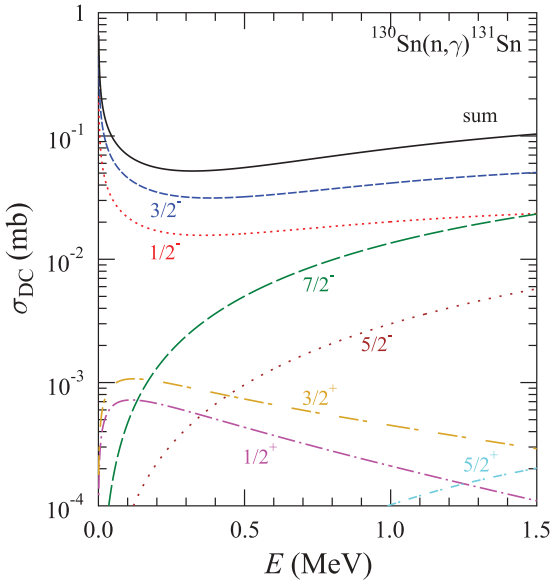

FIG. 2. (Color online) DC cross section of the ^{130}Sn$(n,\gamma)^{131}$Sn reaction. The contributions of the bound states in Table I are shown by colored dashed and dotted lines. The full black line represents the sum over all bound states.

laboratory reaction rate $\mathcal{R}_{\rm lab}$ and the stellar reaction rate $\mathcal{R}^*$ are practically identical in the important temperature range around $T_9 \approx 1$ [25]. The reaction rates of both reactions under study are very similar and show a weak temperature dependence (see Fig. 3). The results can be simply parametrized by a three-parameter parabolic fit

$$\mathcal{R}(T) = N_A \langle \sigma v \rangle \approx \left(a_0 + a_1 T_9 + a_2 T_9^2\right) \frac{\rm cm^3}{\rm s\,mol} \qquad (4)$$

with $a_0 = 16811\,(16321)$, $a_1 = 2291\,(2236)$, and $a_2 = 700\,(870)$ for ^{130}Sn (^{132}Sn). The deviations of the fit are 1–2% over the full temperature range under study.

Uncertainties of the DC cross sections are studied by a variation of the different parameters of the calculation within reasonably estimated ranges and by considering the experimental uncertainties of the bound-state properties. The uncertainty of the neutron separation energies S_n and the excitation energies E_x lead typically to uncertainties for the transition energy E_γ of less than 10%. Together with the E_γ^3 dependence of the $E1$ transition strength a typical uncertainty of about 10–30% is found for the various transitions under study. A variation of the potential geometry (using a larger value of $R_0 = 1.4$ fm instead of $R_0 = 1.25$ fm) and readjustment of the potential depths leads to variations of the DC cross section of between 10–20%. A reduction of the potential depth V_0 by 3% reduces the DC cross section by about 15%. The spectroscopic factors C^2S have uncertainties of about 30% which enter linearly into the DC calculation. By combining all the above uncertainties of the order of 10–30%, a total uncertainty below 50% is a reasonable estimate for the total DC cross section of the ^{130}Sn$(n,\gamma)^{131}$Sn and ^{132}Sn$(n,\gamma)^{133}$Sn reactions.

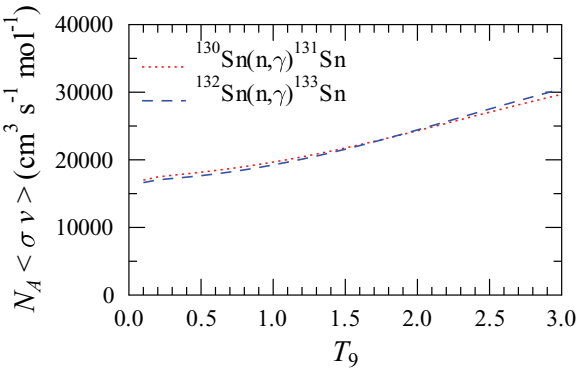

FIG. 3. (Color online) Stellar reaction rate $\mathcal{R}(T) = N_A \langle \sigma v \rangle$ for the ^{130}Sn$(n,\gamma)^{131}$Sn (red dotted line) and ^{132}Sn$(n,\gamma)^{133}$Sn (blue dashed line) reactions.

For the ^{132}Sn$(n,\gamma)^{133}$Sn reaction reasonable agreement with the three predictions in [17] is found whereas the new result is lower by a factor of slightly above 2 (slightly below 2) than the calculation in [13] (Ref. [18]). The energy dependence of all calculations [13,18] is very similar because it is essentially defined by the angular momenta in the entrance channel in combination with the electromagnetic selection rules.

The obtained results for the ^{130}Sn$(n,\gamma)^{131}$Sn reaction are slightly below but very close to the calculations shown in Fig. 4 of [19]. This is not surprising because the same bound-state properties (J^π and E_x) are used. The essential difference between this work and [19] is the replacement of the global optical potential in [19] by the locally optimized potential, which reduces the uncertainties for the calculated $\sigma_{\rm DC}$.

The new $\sigma_{\rm DC}$ for ^{130}Sn$(n,\gamma)^{131}$Sn is about a factor of 2 below the highest result by Rauscher *et al.* [17]. There are two further calculations in [17] with much smaller cross sections, which result from the fact that some of the bound states in Table I are unbound in the corresponding calculations. However, the dramatic reduction of the DC cross section in [17] is an artifact of the separate treatment of the entrance and exit channels. If the $L = 1$ bound states were indeed unbound, the $L = 1$ strength would be located close above threshold and show up as resonances in $\sigma_{\rm DC}$ (and increase $\sigma_{\rm DC}$ via transitions to bound positive-parity states in ^{131}Sn instead of reducing $\sigma_{\rm DC}$). This can be simulated by a reduction of the potential depth V_0, but it is not taken into account in [17] using a fixed potential in the entrance channel. For example, using $V_0 = 41.0$ MeV (instead of 46.2 MeV) leads to a strong $3/2^-$ resonance at about 73 keV with a total width $\Gamma \approx 58$ keV and a total cross section of 4.2 mb in the resonance maximum, i.e., a factor of about 50 higher than the standard calculation shown in Fig. 2. The resulting stellar reaction rate $\mathcal{R}$ becomes temperature-dependent and would be a factor of 10–20 higher than the result in Fig. 3 because of this artificial $3/2^-$ resonance. However, such a strong resonance has been excluded by the transfer data [19].

Finally, predictions of the ^{130}Sn$(n,\gamma)^{131}$Sn and ^{132}Sn$(n,\gamma)^{133}$Sn cross sections from the statistical model have to be discussed briefly. As pointed out, e.g., in [25], the statistical model is not applicable below $T_9 \approx 1.4$ for ^{132}Sn and below $T_9 \approx 0.2$ for ^{130}Sn because the level density is too low. The limit for ^{130}Sn may even be higher if one takes

into account that surprisingly low fragmentation of strength and very similar properties of ^{131}Sn and ^{133}Sn were found in the transfer experiments [19,20]. As a consequence, large deviations are found for predictions from the statistical model using different ingredients (for details see Fig. 1 of [15] and discussion). Thus, a better estimate for resonant contributions might be the procedure of lowering the potential depth V_0 (as outlined above). From the spectroscopic factors in [19] (see also Table I) the missing $\approx$25% of the $L = 1$ or $L = 3$ strengths may be located above threshold but below the detection limit of [19]. A resonance with full $3/2^-$ strength would lead to an enhancement of the stellar reaction rate $\mathcal{R}$ by a factor of 10–20; thus, a weaker resonance with 25% of the strength should enhance $\mathcal{R}$ by not more than a factor of 2.5–5 if located close above the threshold, and the resonant enhancement is decreasing for higher-lying resonances. Such an enhancement is only expected in the ^{130}Sn$(n,\gamma)^{131}$Sn reaction, but not for the ^{132}Sn$(n,\gamma)^{133}$Sn reaction because there are no bound states with positive parity in ^{133}Sn [21,23].

In summary, the direct capture cross section of the ^{130}Sn$(n,\gamma)^{131}$Sn and ^{132}Sn$(n,\gamma)^{133}$Sn reactions has been calculated using local parameters which could be derived mainly from recent (d,p) transfer experiments [19,20]. The DC cross sections of ^{130}Sn and ^{132}Sn are almost identical and could be determined with relatively small uncertainties of less than a factor of 2. Additional resonant contributions may enhance the stellar reaction rate by up to a factor of 5 for ^{130}Sn depending on whether the remaining $L = 1$ and $L = 3$ strength is located in a narrow energy window close above threshold. Huge enhancements of the reaction rate $\mathcal{R}$ of a factor of 10 or even 100 (as discussed in [16]) are excluded by the present study.

This work was supported by OTKA (NN83261).

[1] Y. Nagai, M. Igashira, T. Takaoka, T. Kikuchi, T. Shima, A. Tomyo, A. Mengoni, and T. Otsuka, Phys. Rev. C **71**, 055803 (2005).
[2] T. Kikuchi, Y. Nagai, T. S. Suzuki, T. Shima, T. Kii, M. Igashira, A. Mengoni, and T. Otsuka, Phys. Rev. C **57**, 2724 (1998).
[3] M. Igashira, Y. Nagai, K. Masuda, T. Ohsaki, and H. Kitazawa, Astrophys. J. **441**, 89 (1995).
[4] J. Meissner, H. Schatz, J. Görres, H. Herndl, M. Wiescher, H. Beer, and F. Käppeler, Phys. Rev. C **53**, 459 (1996).
[5] T. Ohsaki, M. Igashira, Y. Nagai, M. Segawa, and K. Muto, Phys. Rev. C **77**, 051303(R) (2008).
[6] H. Beer, P. V. Sedyshev, W. Rochow, P. Mohr, and H. Oberhummer, Nucl. Phys. A **705**, 239 (2002).
[7] A. Tomyo, Y. Nagai, Y. Nobuhara, T. Shima, H. Makii, K. Mishima, and M. Igashira, Nucl. Phys. A **718**, 527 (2003).
[8] P. Mohr, H. Beer, H. Oberhummer, and G. Staudt, Phys. Rev. C **58**, 932 (1998).
[9] P. Mohr, H. Beer, H. Oberhummer, W. Rochow, P. V. Sedyshev, S. Volz, and A. Zilges, Phys. Rev. C **60**, 017603 (1999).
[10] H. Beer, C. Coceva, P. V. Sedyshev, Yu. P. Popov, H. Herndl, R. Hofinger, P. Mohr, and H. Oberhummer, Phys. Rev. C **54**, 2014 (1996).
[11] P. Mohr, H. Oberhummer, H. Beer, W. Rochow, V. Kölle, G. Staudt, P. V. Sedyshev, and Yu. P. Popov, Phys. Rev. C **56**, 1154 (1997).
[12] E. Krausmann, W. Balogh, H. Oberhummer, T. Rauscher, K.-L. Kratz, and W. Ziegert, Phys. Rev. C **53**, 469 (1996).
[13] Y. Xu and S. Goriely, Phys. Rev. C **86**, 045801 (2012).
[14] http://www-nds.iaea.org/amdc/, version amdc.114; G. Audi and W. Meng (private communication).
[15] R. Surman, J. Beun, G. C. McLaughlin, and W. R. Hix, Phys. Rev. C **79**, 045809 (2009).
[16] J. Beun, J. C. Blackmon, W. R. Hix, G. C. McLaughlin, M. S. Smith, and R. Surman, J. Phys. G **36**, 025201 (2009).
[17] T. Rauscher, R. Bieber, H. Oberhummer, K.-L. Kratz, J. Dobaczewski, P. Möller, and M. M. Sharma, Phys. Rev. C **57**, 2031 (1998).
[18] S. Chiba, H. Koura, T. Hayakawa, T. Maruyama, T. Kawano, and T. Kajino, Phys. Rev. C **77**, 015809 (2008).
[19] R. L. Kozub *et al.*, Phys. Rev. Lett. **109**, 172501 (2012).
[20] K. L. Jones *et al.*, Phys. Rev. C **84**, 034601 (2011).
[21] Online database ENSDF, http://www.nndc.bnl.gov/ensdf/.
[22] Y. Khazov, I. Mitropolsky, and A. Rodionov, Nucl. Data Sheets **107**, 2715 (2006).
[23] Y. Khazov, A. Rodionov, and F. G. Kondev, Nucl. Data Sheets **112**, 855 (2011).
[24] S. Goriely, Phys. Lett. B **436**, 10 (1998).
[25] T. Rauscher and F.-K. Thielemann, At. Data Nucl. Data Tables **75**, 1 (2000).